

Under-filling trapping objectives optimizes the use of the available laser power in optical tweezers

Mohammed Mahamdeh,¹ Citlali Pérez Campos,² and Erik Schäffer^{1,*}

¹*Nanomechanics Group, Biotechnology Center, TU Dresden, Tatzberg 47-51, 01307 Dresden, Germany*

²*Max Planck Institute of Molecular Cell Biology and Genetics, Pfotenhauerstraße 108, 01307 Dresden, Germany*

*erik.schaeffer@biotec.tu-dresden.de

Abstract: For optical tweezers, especially when used in biological studies, optimizing the trapping efficiency reduces photo damage or enables the generation of larger trapping forces. One important, yet not-well understood, tuning parameter is how much the laser beam needs to be expanded before coupling it into the trapping objective. Here, we measured the trap stiffness for 0.5-2 μm -diameter microspheres for various beam expansions. We show that the highest overall trapping efficiency is achieved by slightly under-filling a high-numerical aperture objective when using microspheres with a diameter corresponding to about the trapping-laser wavelength in the medium. The optimal filling ratio for the lateral direction depended on the microsphere size, whereas for the axial direction it was nearly independent. Our findings are in agreement with Mie theory calculations and suggest that apart from the choice of the optimal microsphere size, slightly under-filling the objective is key for the optimal performance of an optical trap.

© 2011 Optical Society of America

OCIS codes: (000.2170) Equipment and techniques; (140.7010) Laser trapping; (180.0180) Microscopy; (350.4855) Optical tweezers or optical manipulation.

References and links

1. K. Svoboda and S. M. Block, "Biological applications of optical forces," *Annu. Rev. Biophys. Biomol. Struct.* **23**, 247–285 (1994).
2. N. B. Simpson, D. McGloin, K. Dholakia, L. Allen, and M. J. Padgett, "Optical tweezers with increased axial trapping efficiency," *J. Mod. Opt.* **45**, 1943–1949 (1998).
3. V. Bormuth, A. Jannasch, M. Ander, C. M. van Kats, A. van Blaaderen, J. Howard, and E. Schäffer, "Optical trapping of coated microspheres," *Opt. Express* **16**, 13831–13844 (2008).
4. A. Jannasch, V. Bormuth, C. M. van Kats, A. van Blaaderen, J. Howard, and E. Schäffer, "Coated microspheres as enhanced probes for optical trapping," *Proc. SPIE* p. 70382B (2008).
5. A. Ashkin, "Forces of a single-beam gradient laser trap on a dielectric sphere in the ray optics regime," *Biophys. J.* **61**, 569–582 (1992).
6. H.-I. Kim, I.-J. Joo, S.-H. Song, P.-S. Kim, K.-B. IM, and C.-H. Oh, "Dependence of the optical trapping efficiency on the ratio of the beam radius-to-the aperture radius," *J. Korean Phys. Soc.* **43**(3), 348–351 (2003).
7. M. Bing-Huan, Z. Jin-Hua, Z. Min-Cheng, L. Yin-Mei, W. Jian-Guang, and R. Hong-Liang, "Improvement of transverse trapping efficiency of optical tweezers," *Chin. Phys. Lett.* **25**, 2300–2302 (2008).
8. A. Samadi and N. S. Reihani, "Optimal beam diameter for optical tweezers," *Opt. Lett.* **35**, 1494–1496 (2010).
9. M. Jahnel, M. Behrndt, A. Jannasch, E. Schäffer, and S. Grill, "Measuring the complete force field of an optical trap," *Opt. Lett.* **36**, 1260–1262 (2011).

10. M. Mahamdeh and E. Schäffer, "Optical tweezers with millikelvin precision of temperature-controlled objectives and base-pair resolution," *Opt. Express* **17**, 17190–17199 (2009).
11. A. Pralle, M. Prummer, E. L. Florin, E. H. K. Stelzer, and J. K. H. Hörber, "Three-dimensional high-resolution particle tracking for optical tweezers by forward scattered light," *Microsc. Res. Tech.* **44**, 378–386 (1999).
12. V. Bormuth, J. Howard, and E. Schäffer, "LED illumination for video-enhanced DIC imaging of single microtubules," *J. Microsc.* **226**, 1–5 (2007).
13. D. R. Skinner and R. E. Whitcher, "Measurement of the radius of a high-power laser beam near the focus of a lens," *J. Phys. E: J. Sci. Instrum.* **5**, 237–238 (1972).
14. E. Schäffer, S. F. Nørrelykke, and J. Howard, "Surface forces and drag coefficients of microspheres near a plane surface measured with optical tweezers," *Langmuir* **23**, 3654–3665 (2007).
15. S. F. Tolić-Nørrelykke, E. Schäffer, J. Howard, F. S. Pavone, F. Jülicher, and H. Flyvbjerg, "Calibration of optical tweezers with positional detection in the back focal plane," *Rev. Sci. Instrum.* **77**, 103101 (2006).
16. S. N. S. Reihani and L. B. Oddershede, "Optimizing immersion media refractive index improves optical trapping by compensating spherical aberrations," *Opt. Lett.* **32**, 1998–2000 (2007).
17. N. B. Viana, M. S. Rocha, O. N. Mesquita, A. Mazolli, and P. A. M. Neto, "Characterization of objective transmittance for optical tweezers," *Appl. Opt.* **45**, 4263–4269 (2006).
18. H. van de Hulst, *Light Scattering by Small Particles* (Dover Publications, Inc., 1981).
19. T. A. Nieminen, V. L. Y. Loke, A. B. Stilgoe, G. Knöner, A. M. Brańczyk, N. R. Heckenberg, and H. Rubinsztein-Dunlop, "Optical tweezers computational toolbox," *J. Opt. A, Pure Appl. Opt.* **9**, S196–S203 (2007).
20. V. N. Mahajan, "Uniform versus Gaussian beams - a comparison of the effects of diffraction, obscuration, and aberrations," *J. Opt. Soc. Am. A* **3**, 470–485 (1986).
21. S. Hell, G. Reiner, C. Cremer, and E. H. K. Stelzer, "Aberrations in confocal fluorescence microscopy induced by mismatches in refractive-index," *J. Microsc.* **169**, 391–405 (1993).
22. A. Rohrbach, "Stiffness of optical traps: Quantitative agreement between experiment and electromagnetic theory," *Phys. Rev. Lett.* **95**, 168102 (2005).
23. Note that version 1.0 of the optical tweezers computational toolbox (Ref. [19]) contained a power scaling error in the code which was corrected in version 1.1.
24. J. Pawley, *Handbook of Biological Confocal Microscopy* (Springer, 2006).
25. T. A. Nieminen, H. Rubinsztein-Dunlop, and N. R. Heckenberg, "Multipole expansion of strongly focussed laser beams," *J. Quant. Spectrosc. Radiat. Transf.* **79-80**, 1005–1017 (2003).

1. Introduction

Optical tweezers are sensitive force and position transducers whereby a particle—typically a microsphere acting as a handle and sensor for the experiment of interest—is trapped by a strongly-focused laser beam [1]. When building optical tweezers one eventually needs to decide how much the trapping laser is expanded relative to the size of the trapping objective. If the expansion is too small, the laser focus is not diffraction-limited resulting in smaller stabilizing gradient forces and thus a weaker trap. On the other hand, if the expansion is too large, too much laser power is truncated resulting also in a weak trap. Therefore, there must be an optimal laser expansion to maximize the trap stiffness for a given laser power. Apart from the laser expansion and choice of a high-numerical aperture (NA) objective, the trapping efficiency can also be optimized by using different beam profiles, for instance, a "doughnut" mode [2] or using anti-reflection-coated microspheres [3,4].

Although choosing the optimal expansion is key for making the best use out of the available laser power, previous studies give contradicting recommendations. According to calculations based on ray-optics [1,5] one should slightly *overflow* the objective. Kim *et al.* [6] measured an optimal "laser beam radius-to-the aperture radius" of 1.2 for 5 μm -diameter microspheres in agreement with the ray-optics predictions. In contrast, Bing-Huan *et al.* [7] measured an optimal "effective NA relative to the objective aperture" of 0.7 for 2 μm -diameter microspheres. Recently, Samadi and Reihani [8] measured the optimal "ratio of the beam to the objective's entrance aperture diameter" of about 0.7 for micron-sized microspheres, thus, also recommending *under-filling*. Discrepancies between the studies are due to (i) numerous definitions for the ratio of the beam diameter to some measure of the objective, (ii) different criteria for efficiency (escape force or trap stiffness), (iii) varying microsphere diameters, and (iv) a lack of rigorous Mie theory calculations necessary for particle sizes comparable to the wavelength of light.

Here, we address these points to clarify and reconcile the above-mentioned discrepancies. In addition, we provide information on the axial direction scarcely dealt with previously. Foremost, we introduce a *filling-ratio* parameter which is independent of the objective-back-opening size. The visible stops and apertures in the back of an objective may be larger than the NA of the objective and furthermore depend on the manufacturer. Therefore, we base our filling-ratio parameter on Abbe's sine condition. All high-quality microscope objectives are designed according to this condition to prevent spherical aberrations and coma. Essentially this means that the first principal plane of the objective is a hemisphere (H_1 in inset of Fig. 1(a)). Light rays emerging from the focus under an angle θ relative to the optical axis leave the back of the objective (on the image side) at a radius $r = nf \sin \theta$ where n is the refractive index of the lens and f is the focal length of the objective obtained by dividing the manufacturer's tube length by the magnification of the objective. Note that for large values of θ , common for high-NA objectives, this radius significantly differs from the one obtained with a straight principle plane (for a straight principal plane the radius would scale with $\tan \theta$). Using the definition $NA = n \sin \theta$, the marginal rays that corresponds to the NA of the objective thus span the diameter $D_{NA} = 2fNA$. This diameter in microscopy is also called the exit pupil. Therefore, we define the filling ratio α based on this diameter as

$$\alpha = \frac{2\omega_0}{D_{NA}} = \frac{\omega_0}{fNA} \quad (1)$$

where ω_0 is the laser beam radius at which the intensity decreases to e^{-2} of the central value. If α is multiplied by the NA of the objective, an effective NA can be assigned to the laser beam expansion. This effective numerical aperture in particular the optimal value of it, NA_{opt} is a dimensionless parameter which can be used to compare the performance of different objectives. Here, we determined the optimal filling ratio and thus NA_{opt} for microsphere sizes in the range of 0.5–2 μm using an oil-immersion objective ($NA = 1.3$) and compared the results to Mie theory calculations. As criterion for α , we measured the central trap stiffness since—contrary to the escape force—it is independent of the non-linear trapping force field [9]. We show that slightly under-filling the objective, in our case with $NA_{opt} \approx 1.25$, resulted in the highest trapping efficiency for both lateral and axial directions.

2. Materials and methods

2.1. Optical tweezers setup and laser profile

The setup was described in detail previously [10] except for an exchanged trapping laser (5 W diode-pumped neodymium yttrium vanadate, Nd:YVO₄, infrared laser, $\lambda = 1064 \text{ nm}$; Smart Laser Systems, Berlin, Germany). Briefly, the linearly polarized laser (in the y -direction) was expanded to the desired width using two telescopes: a *three-lens* Galilean telescope for continuously-adjustable expansion and a Kepler telescope with a discrete magnification depending on the choice of lenses. The Kepler telescope was used to increase the limited expansion range of the Galilean telescope. After a change in the expansion, we always realigned the complete laser path. The laser was then coupled into the trapping objective (CFI S Fluor 100 \times /0.7–1.3 NA oil, $f = 2 \text{ mm}$; Nikon, Japan). An identical condenser objective collected the laser light and its back focal plane was imaged onto a quadrant photo-diode (QPD: QP154-Q-HVSD enhanced for 1064 nm detection; Pacific Silicon Sensor, Westlake Village, USA) for microsphere-position detection in three dimensions [11]. For best detection, the condenser and detector were aligned for every sample. The sample itself was mounted on a nanopositioning stage (P-733.3DD, Physik Instrumente, Karlsruhe, Germany). For visualization, we used video-enhanced differential interference contrast with a light emitting diode as a light source (LED-DIC [12]). Images (16 bit with 45 nm pixel size) were captured with a CCD camera (Lm135, Lumenera, Ottawa, Canada). To determine the filling ratio, we measured the laser beam radius

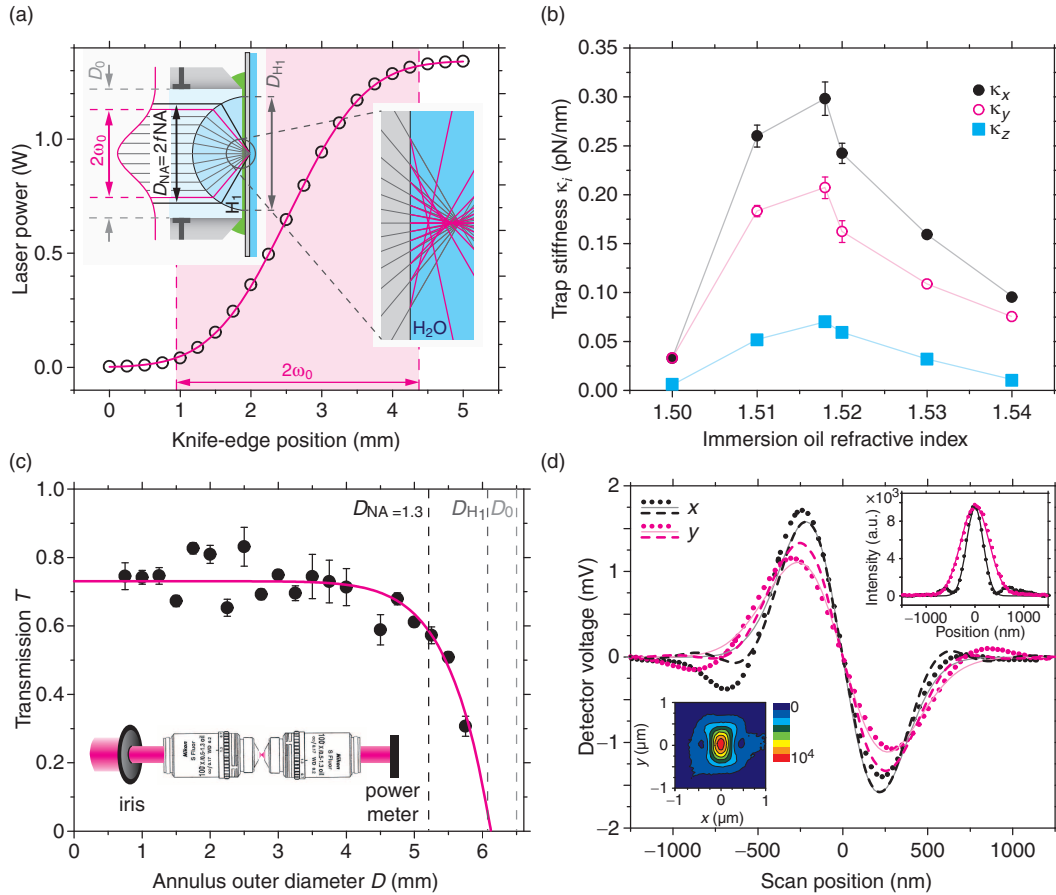


Fig. 1. (a) Exemplary laser profile measured by the knife-edge method. The power measurements (symbols) were fitted with an error function of width $\omega_0 = 1.71 \pm 0.01$ mm. Inset: Schematic objective with a hemispherical principal plane H_1 . Zoom: Aberrations occurring at a glass-water interface when using oil-immersion objectives. The marginal rays correspond to $NA \approx 1.3$, the next ones (spaced by 10°) to $NA \approx 1.15$. (b) Trap stiffness as a function of immersion-oil refractive index for $0.46 \mu\text{m}$ -diameter microspheres. (c) Objective transmission through an annulus with outer diameter D centered on the optical axis. The line is a fit using $T = T_0 - aD^{10}$ with $T_0 = 0.73$ and $a = 10^{-8} \text{ mm}^{-10}$. Inset: Schematic of the measurement (see text for details). For (b) and (c) each symbol is the mean of three measurements. Error bars are standard deviations plotted only if larger than the symbol size. (d) Laser focus profile ($\alpha = 0.95$). Scans (dotted lines) through 80 nm -diameter gold particles fitted to the derivative of a Gaussian ($\omega_{x(y)} = 410(530) \text{ nm}$; dim solid lines) and compared to our calculations ($\omega_{x(y)} = 400(470) \text{ nm}$; dashed lines). The insets show a CCD image of the laser focus and cross-sections (dotted lines; both in the same units) through the center fitted by Gaussians ($\omega_{x(y)} = 340(570) \text{ nm}$; lines).

ω_0 directly before the objective in both the x - and y -direction using the knife-edge method [13] (Fig. 1(a)). All profiles had a Gaussian shape.

2.2. Sample preparation and calibration

The sample was made of two cleaned cover slips ($18 \times 18 \text{ mm}^2$ and $22 \times 22 \text{ mm}^2$, No. 1.5; Corning, NY, USA) glued together by two pieces of double-sided tape leaving a channel of $18 \times 3 \times 0.1 \text{ mm}^3$ in size. The channel was filled with an aqueous solution of polystyrene (PS) microspheres (Bangs Laboratories, Fishers, USA) containing 1 mM KCl. The salt screens repulsive surface forces to less than 100 nm [14] such that microspheres can get into close proximity of the surface but do not get immobilized by the attractive van-der-Waals interactions. To prevent evaporation, the sample was sealed with nail polish.

We calibrated the optical tweezers with a combined drag-force–power-spectral-analysis method using a small sinusoidal lateral stage excitation close to the surface [14, 15]. This method does not require *a priori* knowledge of the viscosity, the microsphere diameter, or the distance to a surface. It provides—apart from the displacement sensitivity of the photo diode and the drag coefficient—the lateral and axial trap stiffness at the surface. The method is suitable for experiments close to a surface because it measures the drag coefficient independently from the other parameters. For every microsphere, we measured all parameters as a function of microsphere–cover-slip distance at ≈ 50 positions starting from a distance of about $3 \mu\text{m}$ until the microsphere touched the surface. From the distance dependence of the drag coefficient, we determined the cover-slip surface position with nanometer precision. For this position, we state the determined trap stiffness [14]. We calibrated at least six different microspheres for each size and filling ratio.

2.3. The optimal immersion oil and uniform objective transmission ensured diffraction-limited performance

Immersion oil. We determined the optimal refractive index of the immersion oil for trapping close to a surface. Reihani and Oddershede [16] reported that an immersion oil with a refractive index of $n = 1.518$, index-matching the cover slip, reduced their trapping efficiency. This was especially the case when working close to the cover glass surface using a $\text{NA} = 1.32$ oil-immersion objective. Using higher refractive-index oils increased their trapping efficiency because spherical aberrations were compensated. Therefore, we measured the trap stiffness as a function of immersion-oil refractive index (Fig. 1(b)). We varied the refractive index in the range of 1.5–1.54 in increments of 0.01 (Series A; Cat.#. 18095; Cargille Laboratories, NJ, USA) including the standard oil we typically use (Immersol, $n = 1.518$; ZEISS, Germany). For all directions, the trap stiffness peaked at the standard oil showing that it is indeed the optimal immersion oil for our setup.

Trapping objective transmission. To compare our measurements with the calculations, we measured the infrared transmission of the trapping objective. This measurement enabled us to calculate the power in the laser focus and account for a potentially non-uniform transmission [17]. Using the two-objective method, we measured the laser transmission as a function of distance from the optical axis (see inset Fig. 1(c)) [17]. We incremented the diameter of a calibrated iris by 0.25 mm. For each increment i , we measured the power before, P_{before} , and after, P_{after} , the identical objectives. We then calculated the transmission of a single objective through an annulus of outer diameter D_i according to $T(D_i) \approx ([P_{\text{after}}(D_i) - P_{\text{after}}(D_{i-1})]/[P_{\text{before}}(D_i) - P_{\text{before}}(D_{i-1})])^{1/2}$. The central transmission was 73 % in very good agreement with the manufacturer's specification (Fig. 1(c)). Also, the transmission was nearly constant up to the diameter corresponding to the objective NA (exit pupil) of $D_{\text{NA}} = 5.2 \text{ mm}$. For larger diameters, the transmission dropped rapidly and was zero at $\approx 6.12 \text{ mm}$ in agreement with the principal-plane diameter $D_{\text{H}_1} = 2n_{\text{oil}}f = 6.07 \text{ mm}$. The visible stop in the back of the objective had a diameter of $D_0 \approx 6.5 \text{ mm}$ (see schematic inset of Fig. 1(a)). Thus, the objective back opening was much larger (about 25 %) compared to the corresponding NA or pupil diameter. Note that significantly

smaller filling ratios result when this stop is used as a reference.

Laser focus. Since our trapping objective is not optimized for the near-infrared, we measured the laser profile in the focal plane to ensure diffraction-limited performance (Fig. 1(d)). We took a camera image of the laser focus reflected from the glass-water interface. In addition, we scanned through gold nanoparticles and recorded the profile with the QPD. Both measurements we compared with the profiles used in the trap stiffness calculations. The measured profiles were asymmetric as expected for a linearly polarized laser and approximately agreed with the calculated size. The beam radius obtained from the gold-nanoparticle scans were 3 % (13 %) larger compared to the theoretical values used in the calculations for the $x(y)$ -direction, respectively. We expected this difference because the laser beam is not a perfect Gaussian beam as characterized by the so-called M^2 value. The diffraction-limited spot size is proportional to this M^2 value. According to the specifications of our laser, $M_{x(y)}^2 = 1.05(1.13)$ for the $x(y)$ -direction, respectively. These values account for the increase in the measured spot size. As an independent visual control, we recorded an image of the laser focused on the cover slip surface. The size determined from cross-sections through the image were 15 % smaller (21 % larger) relative to the theoretical values for the $x(y)$ -direction, respectively. We attribute these differences to polarization effects: before the light reaches the camera it passes a dichroic mirror and several other optics which may have a polarization-dependent transmission. In addition, the camera sensitivity may be polarization-dependent. There were no such uncertainties for the gold-particle scans. Therefore, we assume that the size obtained from the latter data reflect the true size of our laser focus. Taken together, the objective performed nearly diffraction-limited.

3. Results and discussion

3.1. Under-filling resulted in the highest trap stiffness

To determine the optimal filling ratio, we measured the trap stiffness (see Sect. 2) as a function of the filling ratio for four microsphere diameters (0.46, 0.85, 1.01, and 2.01 μm) and seven filling ratios ($\alpha \approx 0.54, 0.67, 0.82, 0.96, 1.15, 1.66$ and 2.25) using a constant laser power before the trapping objective (Fig. 2). From the measurements we can draw the following conclusions: (i) The trap stiffness—for both the lateral and axial directions—was largest at a filling ratio below one, i.e. at under-filling conditions, for all microsphere sizes. (ii) For the lateral directions, the optimal under-filling ratio was size-dependent and decreased with increasing microsphere diameter. For example, the optimal filling ratios for the x -direction were 0.94, 0.94, 0.8 and 0.66 for the four different microsphere sizes, respectively. (iii) For the axial direction, the optimal under-filling ratio was rather size-independent and about 0.95. (iv) As expected [3], the overall highest trap stiffness was achieved with the microspheres that had a diameter of 0.85 μm . This diameter corresponds to about the trapping laser wavelength in the medium, $\lambda/n_{\text{medium}} \approx 800$ nm, where a Mie resonance occurs [18]. During the measurements, we noticed that with filling ratios $\alpha \lesssim 0.9$, the trapping of microspheres became more difficult and the distance from the surface up to which microspheres could still be trapped decreased (to about 5 μm from the cover-slip surface for $\alpha = 0.67$). This effect is due to the low effective NA and the increasing offset between the trap center and the focus (see below and inset Fig. 2(c)). With increasing distance to the surface, spherical aberrations increase. This increase weakens the trap until microspheres cannot be trapped anymore. At the lowest filling ratio of $\alpha = 0.54$ corresponding to an effective NA of 0.7, we were not able to trap any microspheres anymore because the gradient force in the axial direction was too small compared to the scattering force. In summary, the optimal laser expansion depended on the experimental choice of the microsphere size.

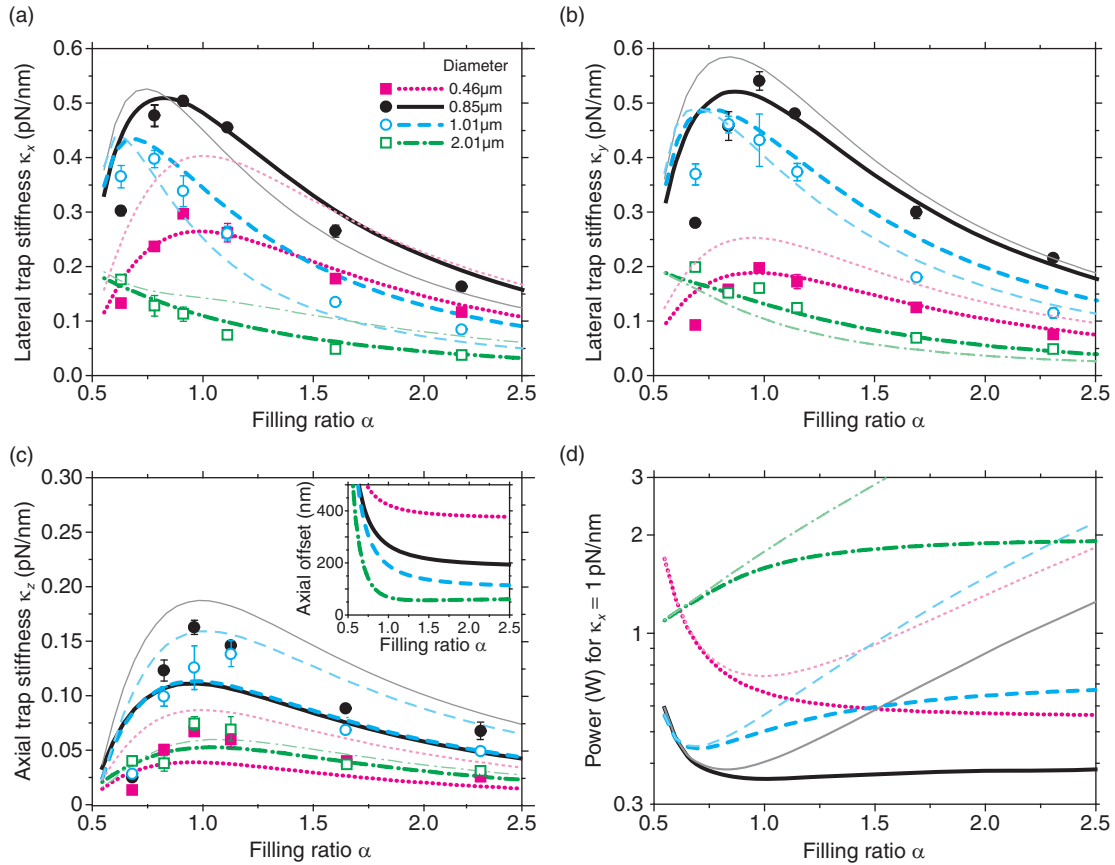


Fig. 2. Trap stiffness measurements (symbols) and calculations (thick [thin] lines for NA = 1.2[1.3]) as a function of filling ratio α for four microsphere sizes in the lateral x - (a), y - (b), and axial z -direction (c). Inset in (c): Axial trap position relative to the center of the focus as a function of filling ratio (NA = 1.2). Symbols are averages obtained from ≥ 6 different microspheres for each size. Error bars are standard deviations plotted only if larger than the symbol size. For all measurements the laser power before the trapping objective was $P = 250$ mW. Due to a 4% asymmetry in the laser profile, overfilling ratios in the y -axis were slightly larger than those in the x -axis. (d) To achieve a trap stiffness of $\kappa_x = 1$ pN/nm, the power in the focus (using our fit parameters; thick lines [NA = 1.2]) and before the objective (assuming 100% transmission; thin lines [NA = 1.2]) are plotted as a function of α .

3.2. Mie theory calculations confirm the under-filling optimum

To compute the trap stiffness, we calculated the light momentum transfer onto the microspheres based on the generalized Lorenz-Mie theory. To this end, we used and extended the optical tweezers computational toolbox [19] to account for (i) the filling ratio, (ii) the spherical principal plane, (iii) the transmission profile of the objective, and (iv) the change in light-ray angles due to the glass-water interface. The latter was implemented based on Snell's law and is approximately valid for water-immersion objectives. A full treatment of aberrations in the case of oil-immersion objectives is not implemented. A detailed description of the modifications to the MATLAB[®] scripts is provided in the Appendix.

We found qualitative agreement between theory and experiment in terms of how the trap

stiffness depended on the filling ratio, microsphere size, polarization, and trapping direction. This agreement confirms the experimental conclusions above. The thick lines in Fig. 2 were obtained with the following parameters: PS microspheres with a refractive index $n_{\text{PS}} = 1.57$ trapped in water, $n_{\text{medium}} = 1.326$, with 1064 nm-light polarized in the y -direction truncated at an angle corresponding to an effective NA of 1.2. For this global fit, we varied only two parameters: the truncation angle, i.e. the effective NA of the objective, and a scaling factor for the effective power in the focus. We found that the effective NA was smaller compared to the oil-immersion objective's specification due to spherical aberrations at the glass-water interface (inset Fig. 1(a)). The theoretical power was significantly lower (scaling factor of 0.62) than our measured power in the focus. To show how the NA affects the shape of the trap stiffness curves, we also calculated the trap stiffness for the objective NA of 1.3 using the same scaling factor of 0.62 (thin lines). The calculations for NA = 1.3 deviated significantly more than the ones for NA = 1.2 indicating that the effective NA of our objective was reduced by the spherical aberrations at the glass-water interface.

Scaling of the trap stiffness with respect to all other parameters agreed qualitatively with the theory, whereas the scaling with power did not. The origin of this discrepancy is unclear, but was observed before [3]. In our present work, we tried to rule out efficiency losses due to (i) the immersion oil (Fig. 1(b)), (ii) the objective transmission (Fig. 1(c)), (iii) a lack of diffraction-limited performance of the objective (Fig. 1(d)), and (iv) calculated power loss in the focus due to diffraction ($<15\%$ for $\alpha = 2.5$, [20]). Note that the power in the focus is deduced from the transmission measurements and not directly measured. How much spherical aberrations from the glass-water interface affect our measurements is unclear as well. Since we work close to this interface ($\lesssim 3 \mu\text{m}$ distance where we measured the trap stiffness), we do not expect that these aberrations fully account for the large difference between theory and experiment [21]. Our measurements, scaled properly, are comparable to other trap stiffness measurements obtained with a water-immersion objective [22]. Whether quantitative agreement between theory and experiments using the optical tweezers computational toolbox can be achieved with an infrared-corrected water-immersion objective is therefore unclear. We do not know of any report that tested the toolbox quantitatively against an optical trapping experiment [23].

While the overall data, apart from the power scaling, qualitatively agreed with the calculations, there were some systematic deviations which we attribute to the aberrations induced by the glass-water interface. These aberrations broaden the focus with increasing surface distance and more so with respect to the axial compared to the lateral direction [21]. Therefore, we expected and observed larger differences between theory and experiment for the axial trap stiffness (Fig. 2(c)). Furthermore, we consistently measured smaller trap stiffness values compared to the theory for small filling ratios. This effect arises because the offset between the axial equilibrium trap position and the laser focus strongly increases for $\alpha < 1$ based on our calculations (inset Fig. 2(c)). This increase is exacerbated by the aberrations mentioned above with the consequence of a systematic weakening of the trap. Overall, our error bars on the trap stiffness measurements were smaller than the mean deviation from the theory, however, considering that with each filling ratio the complete laser path, and with each sample the condenser objective and detector had to be re-aligned, the overall agreement for the range of microsphere sizes and filling ratios is remarkable.

4. Conclusions

For all microsphere sizes, both experiment and calculations show that slight under-filling the objective maximizes the use of the available laser power. At under-filling conditions less power is truncated at the cost of a wider focus due to a lower effective NA. The calculated trap stiffness is the product of the trapping efficiency with the power in the focus. Since the maximum

in trap stiffness occurs at under-filling conditions it means that the power loss due to truncation has a stronger dependence on the filling ratio than the increase in trapping efficiency with respect to a tighter focus. This is expected because power truncation exponentially depends on α [see Eq. (3)] and therefore the effective NA, while the diffraction-limited spot size scales only inversely with the effective NA. One direct consequence of optimizing trapping efficiencies is the reduction of heating and photo-damage in particular when working with biological samples. The least power in the focus to generate a trap stiffness of 1 pN/nm was needed for the 0.85 μm -diameter microspheres for $\alpha = 1$ (≈ 360 mW based on our calculations, black solid line Fig. 2(d)). For the 0.46 μm -diameter microspheres, the power to achieve the same trap stiffness was at least 50 % larger (thick magenta dotted line). The larger the over-filling ratio was for this size, the less power in the focus was necessary. This trend was contrary to the other microsphere sizes we used. For the two large microsphere sizes we tested, under-filling conditions lead to the least power for a 1 pN/nm-trap. When designing optical tweezers, Fig. 2(d) may also serve as a reference for how much output power the laser needs to have. For $\alpha \gtrsim 1$, truncation leads to significant power loss (thin lines). The truncated power may lead to additional heating and thermal drift of the objective [10].

In the light of our results, we can return to the different filling ratio recommendations found in the literature. Using our filling ratio definition [Eq. (1)], Kim *et al.* [6] measured a rather large optimal $\alpha \approx 1.7$ due to aberrations (usage of an oil-immersion objective and trapping ≈ 25 μm away from the surface without refractive index compensation). The optimal value of $\alpha = 0.83$ ($\text{NA}_{\text{opt}} = 1.12$) from Bing-Huan *et al.* [7] is still large compared to our 2 μm -diameter-microsphere measurements. Samadi and Reihani's [8] optimal measured ratio of 0.65 for 0.8 and 1.0 μm -diameter microspheres corresponds to an optimal NA_{opt} of 1.14 and $\alpha = 0.88$ in good agreement with our measurements. Thus, using a reference parameter for the filling ratio which is independent of the objective's back opening size helps in comparing different studies.

For a general, all-purpose usage of the optical tweezers, we recommend a filling ratio slightly below one of $\alpha_{\text{opt}} \approx 0.95$ when using a 1.3 NA-oil-immersion objective. This value corresponds to an optimal filling numerical aperture of $\text{NA}_{\text{opt}} \approx 1.25$. According to our calculations the optimal values for the lateral directions were lower ($\alpha \approx 0.8$, $\text{NA}_{\text{opt}} \approx 1.04$). Therefore, we expect that optimal values for water-immersion objectives with minimized spherical aberrations are lower, in particular for objectives corrected in the near-infrared. As total-internal-reflection-fluorescence (TIRF) objectives are used with immersion oils, we expect that spherical aberrations reduce the effective NA to values comparable to our measurements. Any light rays at radial distances corresponding to NAs larger than the refractive index of the trapping medium cannot contribute to the trap because of total internal reflection. Thus, for TIRF objectives with $\text{NA} \geq 1.4$, optimal under-filling ratios should be less than 0.9 based on $\text{NA}_{\text{opt}} \approx 1.25$.

In summary, the optimal filling ratio will always be a compromise between the lateral and axial direction and the microsphere size. For the axial direction, a filling ratio of $\alpha \approx 1$ is optimal independent of the microsphere size as shown by our data. Additionally it is independent of the NA of the objective based on our calculations (data not shown). In contrast for the lateral direction, under-filling conditions with respect to the definition in Eq. (1) are optimal. What the exact value for the optimal α is, may depend on the microsphere size, whether an oil or a water immersion objective is used, and how well the objective is corrected for the trapping laser wavelength. Based on our experiments and calculations, an under-filling ratio of $\alpha \approx 0.9 \pm 0.05$ is a good compromise for a high-NA objective. The problem of maximizing the trap stiffness for optical tweezers is analogous to minimizing the extent of a laser focus while retaining the most power in case of confocal microscopy or other high-resolution scanning techniques using multi-photon excitation or stimulated emission depletion [24]. For these techniques, optimizing

the filling ratio should also result in maximal performance for a given laser power.

Appendix

To calculate the trap stiffness, we modified the script "bsc_pointmatch_farfield" of the optical tweezers computational toolbox [25]. This script calculates the vector-spherical-wave-functions expansion coefficients of the laser at the focal plane by matching it to a laser profile in the far field. The electrical field E for a radially symmetric profile is expressed in terms of an incoming angle θ instead of a radial coordinate r in accordance with Abbe's condition (see Introduction). Using our definition of the filling ratio [Eq. (1)], we obtain

$$E = \exp\left(\frac{r}{\omega_0}\right)^2 = \exp\left(\frac{2fn_{\text{medium}} \sin \theta}{\alpha D_{\text{NA}}}\right)^2 \quad (2)$$

where θ is in the range of $0-\pi$. Note the usage of the medium refractive index to account for the glass-water interface. To implement laser power losses due to truncation by the objective, the trap stiffness is reduced by multiplying with a power normalization factor

$$P_{\text{trunc}} = T_0 \left[1 - \exp\left(-2 \left[\frac{D_{\text{max}}}{\alpha D_{\text{NA}}}\right]^2\right)\right] \quad (3)$$

assuming a constant transmission T_0 where D_{max} is the largest diameter up to which light is still transmitted. Since we measured the transmission of the objective, we multiplied the Gaussian beam with the fitted transmission curve and integrated the intensity up to the diameter of the principal plane. This changed P_{trunc} slightly compared to the above equation.

Acknowledgments

We thank Christine Kiefer and Marcus Jahnel for comments on the manuscript. The work was supported by the Deutsche Forschungsgemeinschaft (DFG, Emmy Noether Program) and the Technische Universität Dresden.